Dynamics of Cell Membrane Permeabilization by Saponins Using Terahertz Attenuated Total Reflection

Xiujun Zheng, Guilhem Gallot

Manuscript submitted to **Biophysical***Journal*

Article

Dynamics of cell membrane permeabilization by saponins using terahertz attenuated total reflection

Xiujun Zheng[1] and Guilhem Gallot[1,*]

[1]LOB, Ecole polytechnique, CNRS, INSERM, Institut Polytechnique de Paris, Palaiseau, France

[*]Correspondence: Guilhem.Gallot@polytechnique.edu

ABSTRACT Understanding the relevant parameters of the formation of pores during permeabilization is very challenging for medical applications. Several components are involved: the arrival of the permeabilizing molecules to the membrane, the efficiency of pore formation, and the efflux of cytosol molecules. Using attenuated total reflection in the terahertz domain, we studied the dynamics of MDCK cells after permeabilization by saponin molecules. We developed an analytical model taking into account saponin molecules diffusion, cell geometry, cytosol molecules diffusion and pore dynamics. We also studied the effect of possible pore overlapping on the cell membrane, introducing a dimensionless quantity that is the ration between overlapping and diffusive effects. Pores are found to be static within one hour after their creation, hinting that the diffusion of the saponin molecules to the membrane is the limiting factor in our experiments.

SIGNIFICANCE This study is of particular interest for the controlled delivery of specific molecules through the cell membrane, such as in gene therapy, treatment against cancer or biotechnology. It provides original experiments and modeling of detergent permeabilization of cell membrane. In particular, measurements in the terahertz domain demonstrate the probing of cytosol leakage by optical techniques without specific staining nor labelling.

INTRODUCTION

Biological membranes play a major role in the cellular protection as well as in the transport and control of nutrients. Plasma membrane constitutes a fundamental barrier for the entry of hydrophilic molecules into the cell interior. The selective and controlled permeabilization of this barrier is a condition for many biotechnological and medical applications (1–3): cell-based gene therapy, biomanufacture of proteins, vectors or antibodies, regenerative medicine of engineered tissues, disease modelling, treatment against cancer, drug screening as well as diagnostics and analysis. Possible delivered substances are gene editing molecules, DNA, RNA, proteins, metabolites, peptides, membrane impermeable drugs, antibodies, engineered probes, etc. A cell becomes permeable after the weakening of the plasma membrane to the point of creating a pore. The plasma membrane can be disrupted by physical means such as electroporation, mechanical force, optoporation or thermal effect, as well as by biochemical techniques, the most eminent of which being pore-forming toxins and detergents (4). Many active mechanisms exist for repairing the cell membrane after pore formation and they seem to depend relatively little on the origin of the damage whether the source is electrical, mechanical or chemical (5). These mechanisms mostly depend on the pore size, temperature or cell medium. After plasma membrane disruption, the defect evolution is the result of two opposing forces. Surface pressure tends to increase the defect while line tension favors a shrinking of the membrane and a pore reduction (6, 7). In electroporation, pore are typically found to exponentially decrease in a time scale of minutes or tens of minutes (8, 9). Lipidic membrane can exhibit growth or decay of the pores (10), and exponential defects growth are also found in polymer membranes (11). Studying the relevant parameters for pore formation and dynamics are therefore very important for developing pore models and for medical and industrial applications.

Detergents act by solubilizing the components of the membranes. Amphiphilic plant glycosides saponins are the most popular detergents for reversible cell permeabilization. Although the exact mechanisms are still being studied, it is known that saponins interact with membrane cholesterol, making them more specific to cholesterol-rich plasma membranes (1). Detergents can penetrate the lipid bilayer membrane and induce constrains that distort the membrane, then leading to a weakening of the bilayer and the formation of pores (12). To study cell permeabilization, the terahertz domain exhibits many advantages. It is directly sensitive to ions and proteins in solution contrary to the visible domain, absorption is far less important than in the infrared, and it offers better sensitivity than the hyper-frequency domain (13). Recent works demonstrated the possibility to spectroscopically investigate complex systems such as cells and even tissues or small organs (13–17). Using a Terahertz Attenuated Total Reflection (THz-ATR) device designed for biological samples, we demonstrated the possibility to use THz

sensitivity to follow permeabilization dynamics of live monolayer MDCK cells in real time, without any marker or sample preparation (18). The origin of the terahertz contrast was also investigated and was found to be related to the modification of the dielectric constant of liquid water in the presence of solutes such as ions, peptides or proteins (19). Here, using pore creation by saponins, we present measurements in the terahertz domain and an analytical model describing the relevant physical parameters leading to the pore creation and dynamics. In particular, we studied the dynamics of pores after their creation and the competition between pore overlapping and cytosol molecules effusion.

MATERIALS AND METHODS

Cell growth

Madine-Darby Canine Kidney (MDCK) cells are an immortal cell line derived from dog kidney. They are widely used as a model cell line for studies on epithelial polarization and transport, mechanisms of infection, regulation of tight junctions, etc (20). These cells form a typical cuboidal single layer epithelium when grown to confluence, where they display a height of 10 to 12 μm (21). MDCK cells are maintained in DMEM (Dulbecco's Modified Eagle Medium, ThermoFisher: 61965026) supplemented with 10% fetal bovin serum (ThermoFisher: 10500064), 1% penicillin-streptomycin (ThermoFisher: 15140122) at 37°C and 5% CO_2. Cells are isolated with trypsin-EDTA (ThermoFisher: R001100), passed on silicon plate (for experimental purposes) in culture medium and grown until confluence. Half of the layer is kept on the plate while the other half is scratched free as a reference. Before each experiment, the plate is washed with PBS (Phosphate Buffer Saline, ThermoFisher: 20012019) solution and let reach room temperature (21°C) in 3 ml of PBS. Since the plate diameter is 36 mm, the cells are covered by a 3 mm hight of solution. The cells density is about 20000 per cm^2, counted with a Malassez hemocytometer, before culturing during 72±4 h.

Saponin detergent

The saponins are glycosides mainly produced by plants that form soap-like foams in solution. Saponins consist of a sugar moeity linked to a hydrophobic aglycone (22). A great variety of saponins are found, depending on the nature of the aglycone, side chains and relative positions (23). Saponins at high concentration are more commonly used in immunocytochemistry to permeabilize membranes of different kind of fixed cells, but have also been reported to permeabilize live cell plasma membrane

at low concentration and in a reversible way (24). It is a nonionic detergent that creates non-specific pores in cell membrane, most probably by binding with the cholesterol within the lipid components of the cell membrane (22). It can mostly trigger protein and ion transfers through the membrane. Saponin used (SigmaAldrich: 47036) is a mixture of sapogenin molecules at a mass fraction $f = 8$ to 25%, so exact quantity of saponin is unknown. All the experiments were done with the same saponin sample to preserve the direct comparison between the experiments. The saponin number concentration C_0 is related to the mass concentration γ_0 of the commercial saponin as

$$C_0 = \frac{f \mathcal{N}_A \gamma_0}{M} \tag{1}$$

where $\mathcal{N}_A$ is Avogadro constant, and M the molar mass.

Terahertz ATR measurements

Terahertz Attenuated Total Reflection (THz-ATR) makes use of the evanescent wave at the back of a prism under total internal reflection, which is coupled to the sample under study (Fig. 1). When light is reflected at the interface of two optical media with $n_1 > n_2$ total reflection occurs for $n_1 \sin\theta > n_2$ and an evanescent field exists in the less optically dense medium n_2 (Fig. 1b). If an absorbing layer such as cells is put on top of the prism, it couples with the evanescent field and decreases the amount of reflected energy. The measurement of the reflected beam is then directly correlated with the dielectric constant of the medium topping the prism. The penetration depth of the evanescent field depends on the beam wavelength and on the dielectric constants of the prism and of the topping medium. It ranges from 10 to 20 μm in our experimental conditions (25). More precisely, we consider a thin layer of cells and the surrounding solution in this inhomogeneous evanescent wave. Providing that the thickness of the cell layer matches the penetration depth of the evanescent wave, the reflected terahertz wave is modified by the terahertz dielectric properties of the cell layer in contact with the top of the prism. The stronger coupling is obtained for a penetration depth of the same value as the cell layer thickness. The resulting reflected terahertz signal is then correlated with the cytosol content. The extracellular solution above the cell layer only weakly affects the terahertz signal since its volume is much larger than the intracellular one. Therefore, cytosol leakage from the cell to the surrounding solution can easily be detected by the change of the cell content (18, 19).

The terahertz signal is generated by a Terahertz Time-Domain Spectroscopy (THz-TDS) setup (26, 27) composed of a GaAs photoconductive transmitter lit by a femtosecond laser that generates a subsingle cycle THz pulse, with frequencies centered around 0.5 THz and extending from 0.2 to 2 THz. The THz pulse is detected by a low temperature grown GaAs

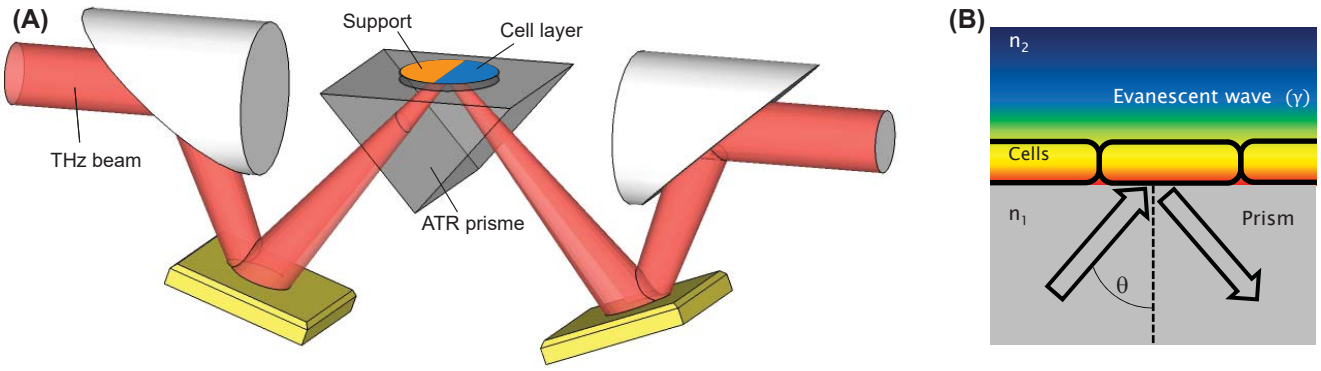

Figure 1: THz-ATR device inserted in the THz-TDS setup. (A) The sample is located on top of a silicon support put in close contact with the top of the silicon prism. The support can be translated. Polarization is in the incident plane (p-polarization). (B) Close view of the ATR prism. The cell layer lyes in the evancescent field zone (in color gradient).

photoconductive detector. A delay line between the emitter and detector terahertz chips allows to measure the amplitude $A(t)$ of the terahertz electric field in the time domain at controlled delay t. An ATR prism (see Fig. 1a) is added to the THz-TDS setup and generates the evanescent wave at its back and senses the cells under study (25). The THz-ATR prism is a very transparent high-resistivity (HR) silicon isosceles prism ($n \approx 3.42$) with a base angle of 42°. The impinging beam is polarized in the plane of incidence (p-polarization). Its reflection depends on both absorption and refractive index of the sample topping the prism. MDCK cells are grown on a HR 3-mm-thick silicon window, put in close contact with the prism to provide optical continuity. Planeity for prism and window surface is better than 1 μm. The window can be translated during data acquisition by a motorized translation stage so that acquisitions can be done either in the cell or reference PBS areas. Peak Amplitude (PA) of $A(t)$ is chosen as it demonstrates the strongest sensitivity between cells and PBS zones (18). We define a relative Δ_{rel} and normalized Δ experimental contrasts

$$\Delta(t) = \frac{\Delta_{\text{rel}}(t)}{\Delta_{\text{rel}}(t=0)} \quad \text{with} \quad \Delta_{\text{rel}}(t) = \frac{\text{PA}_{\text{cell}}(t) - \text{PA}_{\text{ref}}(t)}{\text{PA}_{\text{ref}}(t)}, \tag{2}$$

where PA_{ref} and PA_{cell} are the PA in PBS reference and cell zones, respectively, obtained by moving the sample windows with the motorized translation stage. Perturbation is applied to the cells at time $t = 0$. For each position, the PA value is obtained in 0.25 s. The cell layers typically display a 7 to 8% peak-amplitude relative contrast Δ_{rel} compared to PBS alone.

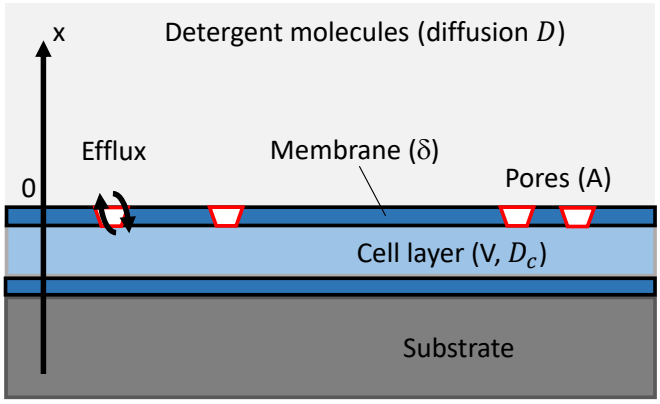

Figure 2: Model of the pore formation mechanism on the cell membrane. The cell layer is put on top of the prism substrate.

Modeling

The system is considered to be a uniform cell layer (see Fig.2). The basal plasma membrane is in contact with the silicon substrate while the apical membrane is in direct contact with saponin molecules in solution in PBS. The saponin molecules can move freely in the liquid by diffusion or sedimentation. Once a molecule encounters the apical membrane it creates a pore with a given probability, increasing the total number of pores with time. Then, effusion of molecules through the pores takes place and changes the concentration of molecules in cytosol. The saponin concentration of the solution is not considered to be modified since the PBS/saponin solution volume is by far much larger than that of cytosol. Pores are allowed to grow or shrink with a characteristic exponential time.

In the following, the model is reduced by symmetry to a 1D-model along the x coordinate. The displacement of saponin molecules of molar mass M is given by the Mason-Weaver equation (28) that describes the diffusion and sedimentation under uniform gravity. In our case, sedimentation is completely negligible compared to diffusion since the convective drag force is much smaller than gravity due to the small size of the saponin molecules. Therefore, the Mason-Weaver equation reduces to the classic diffusion equation

$$\frac{\partial C(x,t)}{\partial t} = D\frac{\partial^2 C(x,t)}{\partial x^2} \tag{3}$$

where $C(x,t)$ is the saponin number concentration at position x and time t, and D the diffusion constant of saponins in PBS. For a semi-infinite volume above the uniform cell surface and the apical membrane plane at $x = 0$, the solution of Eq. 3 for an initial concentration C_0 at time $t = 0$ is

$$C(x,t) = C_0 \,\mathrm{erf}\left(\frac{x}{2\sqrt{Dt}}\right), \tag{4}$$

with erf(x) the error function. For a cell surface A, the total number of molecules impinging the surface is then

$$N_0(t) = A \int_0^\infty [C_0 - C(x,t)] \ \mathrm{d}x = \frac{2A\,C_0\sqrt{Dt}}{\sqrt{\pi}} = \alpha\sqrt{t}. \tag{5}$$

After creation, each pore with initial surface S_{p0} can exponentially increase in size as $S_p(t) = S_{p0}\, e^{t/\tau}$ or exponentially decay as $S_p(t) = S_{p0}\, e^{-t/\tau}$ with τ the characteristic time. At this point, we consider that there is no overlapping of the created pores, so that the number of pores is equal to $\eta\, N_0(t)$ where η is the efficiency of the saponin molecules to create a hole. We introduce the rate of creation of pores

$$j(t) = \eta \frac{dN_0(t)}{dt}. \tag{6}$$

The total surface of pores $\Sigma_p(t)$ for $t > 0$ is given by the convolution between the rate of creation of pores $j(t)$ and the individual surface pore $S_p(t)$ as

$$\Sigma_p(t) = \int_0^t j(u)\ S_p(t-u)\ \mathrm{d}u. \tag{7}$$

The created pores allow effusion of molecules from cytosol according to Fick's first law (29). The number N_c of exiting molecules from cytosol is then

$$\frac{\mathrm{d}N_c(t)}{\mathrm{d}t} = -\gamma(t)\, N_c(t) \quad \text{with} \quad \gamma(t) = \frac{\Sigma_p(t)\, D_c}{V\delta} \tag{8}$$

being the effusion rate, for a cell volume V, with D_c the diffusion constant of molecules in cytosol and δ the plasma membrane thickness. We also define L as the cell thickness so that $V = A\,L$. After some calculations using equations 5, 7 and 8, one obtains an analytical solution for the normalized evolution of the number of molecules leaking the cytosol for increasing or decaying pore sizes, N_{Inc} and N_{Dec}, respectively,

$$\frac{N_{\mathrm{Inc}}(t)}{N_{c0}} = \exp\left\{-\varphi\,\tau^{3/2}\left[\frac{\sqrt{\pi}}{2}\exp\left(\frac{t}{\tau}\right)\mathrm{erf}\sqrt{\frac{t}{\tau}} - \sqrt{\frac{t}{\tau}}\right]\right\} \tag{9}$$

$$\frac{N_{\mathrm{Dec}}(t)}{N_{c0}} = \exp\left\{-\varphi\,\tau^{3/2}\left[\frac{\sqrt{\pi}}{2}\exp\left(\frac{t}{\tau}\right)\mathrm{erfi}\sqrt{\frac{t}{\tau}} - \sqrt{\frac{t}{\tau}}\right]\right\} \tag{10}$$

with

$$\varphi = \frac{2\eta\, C_0 S_{p0} D_c \sqrt{D}}{\sqrt{\pi} L\delta} \tag{11}$$

and with erf(x) the error function, erfi $= -i\,\mathrm{erf}(ix)$ the imaginary error function, and N_{c0} the initial number of molecules in cytosol. Therefore, the population evolution of the lost cytosol molecules depends on two parameters: the exponential pore size evolution time τ and a term φ depending on the diffusion constants D_c and D, on the initial saponin concentration C_0, on the

cell geometry parameters L and δ, and on the pore parameters S_{p0} and η. We can notice that the limits of $N_{\text{Inc}}(t)$ and $N_{\text{Dec}}(t)$, for static pores ($1/\tau \to 0$), are both equal to

$$N_{c0} \exp\left[-\frac{2}{3}\varphi\, t^{3/2}\right]. \tag{12}$$

We now consider the possible overlapping of the pores during their creation from detergent molecules. Without overlapping, the total surface would continuously increase toward infinity (see Eq. 5), which is not physically relevant. In reality, the total surface of the pores is limited by the available membrane surface. We will analytically treat the limit case of static pores ($1/\tau \to 0$). Let us assume that a surface $\Sigma_p(t)$ of pores was created at the surface membrane. The increase of surface $d\Sigma_p(t)$ is given by the surface ration probability $S_{p0}\left[1 - \frac{\Sigma_p(t)}{A}\right]$, so one obtains the differential equation for the pore surface evolution considering pore overlapping

$$\frac{\Sigma_p(t)}{dt} = j(t)\, S_{p0}\left[1 - \frac{\Sigma_p(t)}{A}\right]. \tag{13}$$

Using Eq. 5, the solution of the previous differential equation is, for $t > 0$

$$\Sigma_p(t) = \eta A\left[1 - \exp\left(-\frac{S_{P0}}{A}\alpha\sqrt{t}\right)\right]. \tag{14}$$

Furthermore, the leakage of cytolsol molecules is again calculated using Eq. 8, and we obtain the evolution of the number $N(t)$ of molecules leaking the cytosol, considering overlaping, for static pores

$$\frac{N(t)}{N_{c0}} = \exp\left\{-\frac{\varphi}{f\alpha}\left[t - \frac{1 - e^{-f\alpha\sqrt{t}}\left(1 + f\alpha\sqrt{t}\right)}{\frac{1}{2}f^2\alpha^2}\right]\right\} \tag{15}$$

with $f = S_{p0}/A$. Here, two mechanisms are opposing. The first is the overlapping of the pores which results in a decrease of the total pore surface created by the detergent molecules as well as the saturation of the surface to long delays. Its characteristic time is given by Eq. 14 as $t_1 = \left[A/(S_{p0}\,\alpha)\right]^2$. The second mechanism is the leakage of the cytosol molecules through the pores due to diffusion and pore size evolution. Equation 12 provides the characteristic time $t_2 = (2\varphi/3)^{-2/3}$. We then define a dimensionless number

$$G = \left(\frac{t_2}{t_1}\right)^{3/2} = \frac{6S_{p0}^2 C_0^2 DL\delta}{\pi D_c}. \tag{16}$$

Therefore, if $G \gg 1$ ($t_1 \ll t_2$), the limiting factor is the overlapping of the pores, which takes place before the drop of the molecules inside the cell. The effusion rate is then approximately constant. On the contrary, if $G \ll 1$ ($t_1 \gg t_2$), the limiting factor is the diffusion of the cytosol molecules. Hence, the overlapping plays no role. We can notice that $G \propto \dfrac{D}{D_c}$ which is expected since D_c is related to the diffusion of the effusing molecules while D to the detergent molecules digging the pores.

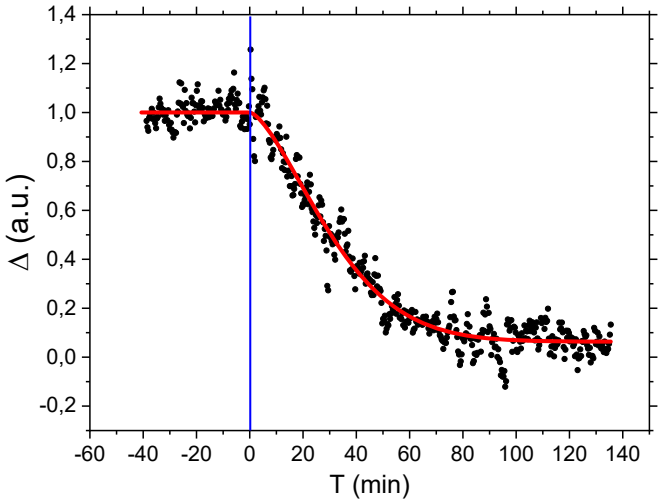

Figure 3: THz-ATR signal $\Delta(t)$ for MDCK cell layer after addition of saponins at $T = 0$ for experimental data (black dots) and best fit (red line). The blue vertical line shows addition of saponin.

For instance, if the diffusion of the cytosol molecules is much smaller than that of the detergent molecules, the leakage of the cytosol molecules would remain in the initial linear regime when the overlapping effects begin to be significant.

Finally, using the dimensionless number G, Eq. 15 rewrites in a more compact form as

$$\frac{N(t)}{N_{c0}} = e^{3/G} \exp\left[-\frac{Dc\ t}{L\delta} - \frac{3}{G}\left(1 + \sqrt{\frac{t}{\tau_G}}\right) e^{-\sqrt{\frac{t}{\tau_G}}}\right] \quad \text{with} \quad \tau_G = \frac{\pi}{4S_{p0}^2 C_0^2 D}. \tag{17}$$

RESULTS AND DISCUSSION

We experimented the effect of the initial concentration of saponins on the membrane permeability dynamics probed by THz-ATR. Before each experiment, the cell support is washed with PBS. For each measurement targetting a given concentration of saponins, a fresh solution of saponin 100 times more concentrated is prepared. The support is put on the THz-ATR prism and let reach room temperature during 15 min at 21°C in 3 ml of PBS. Since the support diameter is 36 mm, the cells are covered by a 3 mm hight of solution. Experiments refer to time T following a perturbation applied to the cells at $T = 0$. We record the THz-ATR signal Δ for 30 min to make sure the signal is stable. Then, at $T = 0$ we add 30 μL of 100X-concentrated solution of saponins in PBS with a micropipette so that the resulting saponins concentration equals γ_0. The liquid is pumped in and out several times to homogenize the solution. Then, the THz signal is further recorded during 120 to 150 min. Typical result versus T is given in Fig.3. Using least square regression, the experimental data are fitted with both Eqs. 9 and 10, considering the

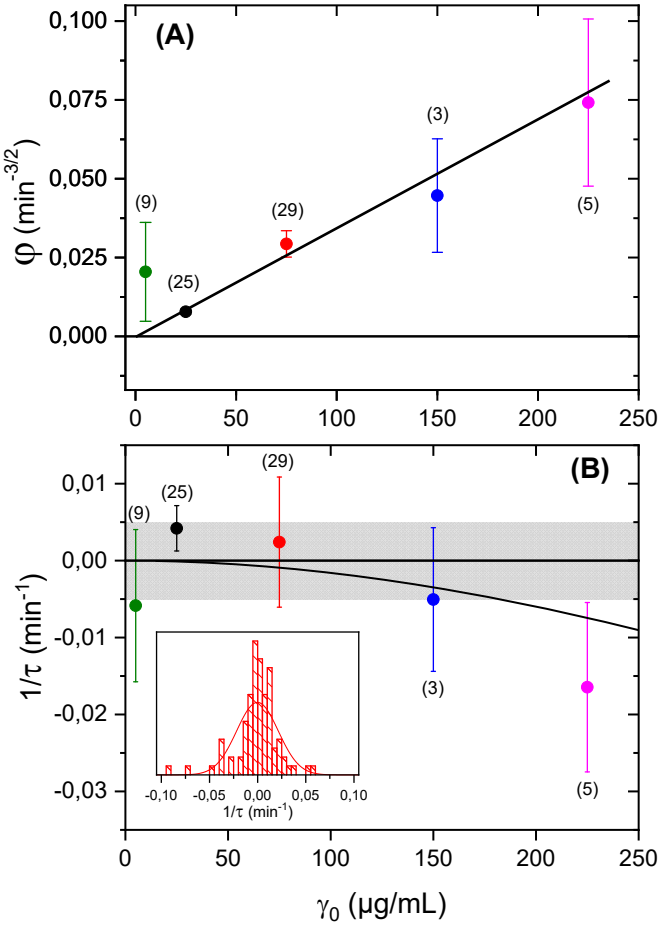

Figure 4: Model parameters φ **(A)** and $1/\tau$ **(B)** versus saponin mass concentration γ_0. **(A)** The line is the best fit proportional function. **(B)** The grey rectangle is a guide for the eye. The black line is the apparent $1/\tau$ evolution considering overlapping of the pores. Inset shows the distribution of $1/\tau$ for the whole concentrations and a Gaussian fit. For both, the number of experiments are shown in parenthesis.

cases of either pore size increase or decay. The best result from these two equations (see the red curve in Fig.3) provides the parameters τ and φ. In the particular case of parameter τ, we attributed by convention a positive sign if the best fit is obtained from Eq. 9 (size increase), or a negative sign if obtained from Eq. 10 (size decay).

We recorded the THz-ATR dynamics of MDCK cells permeabilization after addition of saponins versus mass concentration γ_0. The results are presented in Fig. 4A for parameter φ, and Fig. 4B for parameter $1/\tau$. First, for the cell geometry and diffusion parameter φ, a linear dependency versus γ_0 is experimentally observed, as expected from Eqs. 1 and 11. Precision at lower concentration ($\gamma_0 = 5$ μg/mL) is weaker since the amplitude of variation of THz-ATR signal was lower. The slope obtained

from Fig. 4A is related to Eqs. 1 and 11 as

$$\frac{\varphi}{\gamma_0} = \frac{2N_A f D_c \sqrt{D}}{\sqrt{\pi} M L \delta} \eta S_{p0}. \tag{18}$$

One finds experimentally that $\varphi/\gamma_0 \approx 7.1 \times 10^{-7}$ $\mathrm{m^3 g^{-1} s^{-3/2}}$. Using Eq. 18 and the values found in the Appendix A, one obtains $\eta S_{p0} \approx 2.3 \cdot 10^{-5}$ $\mathrm{nm^2}$ (with $f = 0.12$).

In conjunction with an estimate of the size of the micelle-like pore structure formed by saponin in the bonding with cholesterol molecules (22), one can estimate the diameter of the pores to about 4 nm (30), thus the pore surface to $S_{p0} = 12.5$ $\mathrm{nm^2}$. Assuming a transverse extension of saponin molecule of 0.6 nm (22), about 20 saponin molecules are found in average in the ring. Then, efficiency $\eta \approx 1.8 \cdot 10^{-6}$ to form the 20-molecule ring. Assuming an individual probability p for a saponin molecule to bind to the membrane, one finds $p^{20} = 1.8 \cdot 10^{-6}$ and then $p \approx 52 \pm 2\%$ considering the uncertainty on the commercial concentration of saponin molecules. This shows that the binding probability to the membrane is very high for the saponin molecules.

Second, we studied the variation of the pore size evolution characteristic time (see Fig. 4B). At first sight, $1/\tau$ is very close to 0 within experimental uncertainty, shown in grey in Fig. 4B. This corresponds to $|1/\tau| < 0.05$ $\mathrm{min^{-1}}$ and then to $|\tau| > 200$ min. This means that pores created by saponins exhibit a very slow dynamics if any, longer then 200 min in any case. Furthermore, Fig. 4B seems to exhibit a small descrepency with respect to purely static pores, for larger saponins concentration. The experimental values of $1/\tau$ are slightly negative for high saponins concentrations which would evoque a large but not infinite decaying pore size time. However, this appears to be an artefact due to pore overlapping, as shown by the black line, which is the apparent $1/\tau$ evolution considering pore overlapping. This line is obtained fitting the evolution of the number of leaking cytosol molecules with overlapping and $1/\tau \to 0$ (Eq. 17) by the number of molecules without overlapping (Eq. 10). The overall result is then fully compatible with static pores created by saponin molecules. Due to partial overlopping, the total pore surface becomes slightly smaller than expected, leading to an apparent decay of the pore size. Using the data in Appendix A, one obtains the dimensionless number $G = 1.9 \times 10{-}6 \ll 1$. This confirms that the limiting factor in our experiments is not the overlapping of pores but essentially the effusion process.

CONCLUSION

Using terahertz ATR measurements, we followed the leakage of cytosol molecules after permeabilization by saponin molecules. We elaborated a theoretical model involving saponin molecules diffusion, cell geometry, cytosol molecules diffusion and

Table 1: List of parameter values. (*) confocal microscopy measurements. (**) SigmaAldrich: 47036.

Parameter	Symbol	Value	Unit	Ref.
Cell height	L	10	μm	(*)
Membrane thickness	δ	4	nm	(31)
Cytosol diffusion	D_c	1	$\mu m^2/s$	(32)
Viscosity (water, 300 K)	μ	10^{-3}	Pa.s	(33)
Protein density	ρ	1.37		(34)
Saponin molar mass	M	1200	g/mol	(**)
Saponin fraction	f	8-25%		(**)

pore dynamics, which analytically provides the evolution equations for the cytosol molecules efflux that depends only on two parameters, one relying of the diffusion and cell geometry parameters, and the second to the characteristic evolution time of the created pores. Taking into account overlapping, we also found that two effects are opposing during permeabilization: the pore overlapping related to saponin molecules diffusion, and the efflux dynamics of cytosol molecules. The balance between these two mechanisms can be described introducing a dimensionless number. We found a good correlation between the experimental data and the model. In particular, we found that the pores created by saponin molecules appear to be static within experimental uncertainty, and that the probability for a saponin molecule to bind to the membrane is found to be very efficient, with a probability greater than 50%. Therefore, the most limiting parameter in the MDCK permeabilization by saponin molecules is the diffusion of saponin molecules.

APPENDIX A

We present here the relevent parameters (See Table 1) for the model. Furthermore, the diffusion constant D of saponin molecules in the extracellular domain is given by the Stokes-Einstein equation

$$D = \frac{k_B T}{6\pi\mu r_s} \tag{19}$$

where the Stokes radius r_s is related to the molar mass M of the saponin molecules by

$$r_s = \left[\frac{3M}{4\pi\rho N_A}\right]^{1/3} \tag{20}$$

where $\mathcal{N}_A$ is Avogadro constant. One obtains $D \approx 330\ \mu\text{m}^2/\text{s}$.

AUTHOR CONTRIBUTIONS

X. Zheng carried out all experiments, G. Gallot designed the research, carried out the modelization and wrote the article.

REFERENCES

1. Stewart, M. P., A. Sharei, X. Y. Ding, G. Sahay, R. Langer, and K. F. Jensen, 2016. In vitro and ex vivo strategies for intracellular delivery. *Nature* 538:183–192.

2. Hapala, I., 1997. Breaking the Barrier: Methods for Reversible Permeabilization of Cellular Membranes. *Critical Reviews in Biotechnology* 17:105–122.

3. Eeman, M., and M. Deleu, 2010. From biological membranes to biomimetic model membranes. *Biotechnol. Agron. Soc. Environ.* 14:719–736.

4. Ros, U., and A. J. Garcia-Saez, 2015. More Than a Pore: The Interplay of Pore-Forming Proteins and Lipid Membranes. *Journal of Membrane Biology* 248:545–561.

5. Cooper, S. T., and P. L. McNeil, 2015. Membrane Repair: Mechanisms and Pathophysiology. *Physiological Reviews* 95:1205–1240.

6. Poellmann, M. J., and R. C. Lee, 2017. Repair and Regeneration of the Wounded Cell Membrane. *Regenerative Engineering and Translational Medicine* 3:111–132.

7. Rosetti, C. M., G. G. Montich, and C. Pastorino, 2017. Molecular Insight into the Line Tension of Bilayer Membranes Containing Hybrid Polyunsaturated Lipids. *J Phys Chem B* 121:1587–1600.

8. Breton, M., and L. M. Mir, 2018. Investigation of the chemical mechanisms involved in the electropulsation of membranes at the molecular level. *Bioelectrochemistry* 119:76–83.

9. Teissie, J., M. Golzio, and M. P. Rols, 2005. Mechanisms of cell membrane electropermeabilization: a minireview of our present (lack of ?) knowledge. *Biochim Biophys Acta* 1724:270–80.

10. Ryham, R., I. Berezovik, and F. Cohen, 2011. Aqueous Viscosity Is the Primary Source of Friction in Lipidic Pore Dynamics. *Biophysical Journal* 101:2929–2938.

11. Debregeas, G., P. Martin, and F. Brochard-Wyart, 1995. Viscous bursting of suspended films. *Phys Rev Lett* 75:3886–3889.

12. Islam, M. Z., S. Sharmin, M. Moniruzzaman, and M. Yamazaki, 2018. Elementary processes for the entry of cell-penetrating peptides into lipid bilayer vesicles and bacterial cells. *Applied Microbiology and Biotechnology* 102:3879–3892.

13. Masson, J. B., M. P. Sauviat, J. L. Martin, and G. Gallot, 2006. Ionic contrast terahertz near field imaging of axonal water fluxes. *Proc Natl Acad Sci U S A* 103:4808–4812.

14. Shiraga, K., Y. Ogawa, T. Suzuki, N. Kondo, A. Irisawa, and M. Imamura, 2014. Characterization of Dielectric Responses of Human Cancer Cells in the Terahertz Region. *Journal of Infrared Millimeter and Terahertz Waves* 35:493–502.

15. Yu, C., S. Fan, Y. Sun, and E. Pickwell-MacPherson, 2012. The potential of terahertz imaging for cancer diagnosis: A review of investigations to date. *Quant Imaging Med Surg* 2:33–45.

16. Woodward, R. M., B. E. Cole, V. P. Wallace, R. J. Pye, D. D. Arnone, E. H. Linfield, and M. Pepper, 2002. Terahertz pulsed imaging in reflection geometry of human skin cancer and tissue. *Physics in Medecine and biology* 47:3853–3863.

17. Masson, J.-B., M.-P. Sauviat, and G. Gallot, 2006. Ionic contrast terahertz time resolved imaging of frog auricular heart muscle electrical activity. *Appl. Phys. Lett.* 89:153904.

18. Grognot, M., and G. Gallot, 2015. Quantitative measurement of permeabilization of living cells by terahertz attenuated total reflection. *Appl. Phys. Lett.* 107:103702.

19. Grognot, M., and G. Gallot, 2017. Relative Contributions of Core Protein and Solvation Shell in the Terahertz Dielectric Properties of Protein Solutions. *J. Phys. Chem. B* 121:9508–9512.

20. Lang, F., and M. Paulmichl, 1995. Properties and regulation of ion channels in MDCK cells. *Kidney Int.* 48:1200–1205.

21. Puliafito, A., L. Hufnagel, P. Neveu, S. Streichan, A. Sigal, D. K. Fygenson, and B. I. Shraiman, 2012. Collective and single cell behavior in epithelial contact inhibition. *Proc Natl Acad Sci U S A* 109:739–744.

22. Francis, G., Z. Kerem, H. P. Makkar, and K. Becker, 2002. The biological action of saponins in animal systems: a review. *Br J Nutr* 88:587–605.

23. Fleck, J. D., A. H. Betti, F. P. da Silva, E. A. Troian, C. Olivaro, F. Ferreira, and S. G. Verza, 2019. Saponins from Quillaja saponaria and Quillaja brasiliensis: Particular Chemical Characteristics and Biological Activities. *Molecules* 24.

24. Wassler, M., I. Jonasson, R. Persson, and E. Fries, 1987. Differential permeabilization of membranes by saponin treatment of isolated rat hepatocytes. *Biochem. J.* 247:407–415.

25. Wojdyla, A., and G. Gallot, 2013. Attenuated internal reflection terahertz imaging. *Opt. Lett.* 38:112–114.

26. Grischkowsky, D., S. R. Keiding, M. van Exter, and C. Fattinger, 1990. Far-infrared time-domain spectroscopy with terahertz beams of dielectrics and semiconductors. *J. Opt. Soc. Am. B* 7:2006–2015.

27. Podzorov, A., and G. Gallot, 2008. Low-loss polymers for terahertz applications. *Appl. Opt.* 47:3254–3257.

28. Mason, M., and W. Weaver, 1924. The Settling of Small Particles in a Fluid. *Physical Review* 23:412–426.

29. Crank, J., 1975. The mathematics of diffusion. 2nd edition. Clarendon press, Oxford.

30. Seeman, P., D. Cheng, and G. H. Iles, 1973. Structure of membrane holes in osmotic and saponin hemolysis. *The journal of cell biology* 56:519–527.

31. Mitra, K., I. Ubarretxena-Belandia, T. Taguchi, G. Warren, and D. M. Engelman, 2004. Modulation of the bilayer thickness of exocytic pathway membranes by membrane proteins rather than cholesterol. *Proc Natl Acad Sci U S A* 101:4083–8.

32. Kumar, M., M. S. Mommer, and V. Sourjik, 2010. Mobility of cytoplasmic, membrane, and DNA-binding proteins in Escherichia coli. *Biophys J* 98:552–9.

33. 2004. CRC Handbook of chemistry and physics 84th edition. CRC press.

34. Hinz, H.-J., 1986. Thermodynamic Data for Biochemistry and Biotechnology. Springer-Verlag Berlin Heidelberg.